This document is published in:

Chemical Engineering Journal 215–216 (2013) 15 January, pp. 479–490

DOI:10.1016/j.cej.2012.10.056

Gas interchange between bubble and emulsion phases in a 2D fluidized bed as revealed by two-fluid model simulations

F. Hernández-Jiménez [a,*], A. Gómez-García [a], D. Santana [a], A. Acosta-Iborra [a]

[a] *Universidad Carlos III of Madrid, Department of Thermal and Fluid Engineering, Av. de la Universidad, 30, 28911 Leganés, Madrid, Spain*

Graphical abstract:

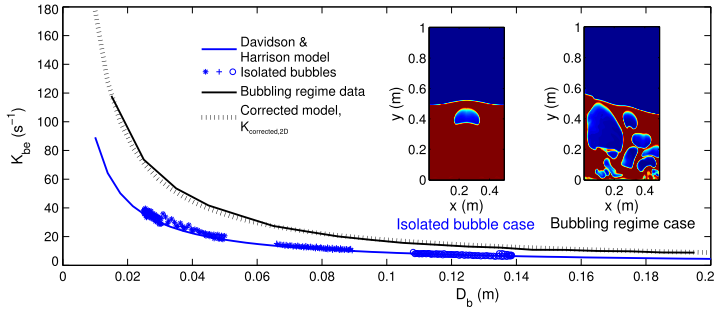

Abstract: Using two fluid model simulations, the present work aims at characterizing the interchange due to gas advection between the emulsion phase and bubbles in fully bubbling beds of Geldart group B particles that are fluidized with air. In the studied beds the bubbles are slow, which means that the advection transport of gas through the bubble boundary is the main mechanism of gas interchange. In an initial ver ification step, the pressure distribution and the gas interchange coefficient for isolated bubbles obtained in the two fluid simulation are compared with the classical potential flow theory of fluidized beds, pro viding concordant results. In a second step, the work analyzes the gas interchange in fully bubbling beds and the effects of the superficial velocity, bed height, and particle diameter on the interchange coefficient and the crossflow ratio. The results indicate that both the interchange coefficient and the crossflow ratio in bubbling beds are about two times those predicted by the potential theory of isolated bubbles. A cor rected model for the gas interchange is proposed based on the introduction of the gas throughflow into the classical potential flow theory. As a consequence, the gas interchange coefficient in the corrected model is a function of the superficial gas velocity instead of the minimum fluidization velocity.

Keywords: Fluidized bed, CFD, Gas interchange, Bubble, Throughflow.

1. Introduction

Fluidized beds have many relevant applications in industry, including, for example, fluid catalytic cracking (FCC), gasification, combustion of solid fuels, and Fischer Tropsch synthesis [1]. De spite the fact that fluidized beds have been used in industry since the 1920s and good progress has been made in the experimental and simulation analysis of these systems, some aspects of fluidized bed dynamics are still far from fully understood.

Especially crucial for the understanding and control of fluidized bed combustors, gasifiers, and other reactors, is the characteriza tion of the gas interchange between the emulsion of particles (i.e. the dense phase) and large voids (i.e. bubbles) in the bed. Simultaneous measurement of both the gas and the particle veloc ities in real beds entails serious difficulties that have not been sat isfactorily solved at present. Thus, detailed numerical modeling of the bubbling process constitutes a valuable tool that can provide complete information of the gas dynamics within the fluidized bed.

* Corresponding author. Tel.: +34 91 624 6032.
E-mail address: fhjimene@ing.uc3m.es (F. Hernández-Jiménez).

Nomenclature

a	isolated bubble radius (m)
c_1, c_2	coefficients for the bubble velocity ( )
D_b	bubble equivalent diameter (m)
d_p	particle diameter (mm)
H	height (m)
H_0	static bed height (m)
K_{be}	interchange coefficient (s^{-1})
K_{gs}	gas solid momentum exchange ( )
U	superficial gas velocity (m/s)
U^*	corrected velocity (m/s)
U_{mf}	minimum fluidization velocity (m/s)
$\vec{g}$	gravity vector (m/s^2)
P	pressure (Pa)
ΔP_g	relative pressure of the gas (Pa)
V_b	bubble volume (m^3)
$\dot{V}_{be}$	volumetric gas flow rate (m^3/s)
$\vec{v}_b$	bubble velocity (m/s)
$\vec{v}_g$	gas velocity (m/s)
$\vec{v}_s$	solids velocity (m/s)
$v_{b,b}$	bubble velocity for bubbling beds (m/s)
$v_{b,i}$	bubble velocity for isolated bubbles (m/s)
W	bed width (m)
X	crossflow ratio ( )
x	horizontal coordinate (m)
x_c	x referred to the bubble centroid (m)
y	vertical coordinate (m)
y_c	y referred to the bubble centroid (m)
Z	2D bed thickness (m)

Greek letters

α_s	solids volume fraction ( )
α_g	voidage ( )
δ	throughflow concentration parameter ( )
ϕ	coefficient for the bubble velocity ( )
ρ_d	bulk density (kg/m^3)
ρ_s	solids density (kg/m^3)
ρ_g	gas density (kg/m^3)
Ψ	fraction of visible bubble flow ( )
Θ	granular temperature (J/kg)
ζ	coefficient for the corrected model ( )

The experimental works available in the literature studying the gas interchange reflect the mentioned difficulties in the measure ment of the gas phase transport in such systems. Most of these works are strongly influenced by the potential flow theory devel oped in the early 1960s by Davidson and Harrison [2] to calculate the volume of gas going in and out of an isolated bubble.

Experimental investigations on the gas interchange can be clas sified into two categories: single bubbles and freely bubbling beds. In both categories the experimental technique employed is usually the analysis of the variation of a tracer concentration with time [3 7]. For example, Sit and Grace [3,4] measured the concentration of ozone in a two dimensional bed and estimated the overall mass transfer coefficient in pairs of coalescence bubbles that were con secutively injected. Wu and Agarwal [7] studied the effect of the temperature on the mass transfer coefficient using single bubbles containing Argon. They found a decrease in the mass transfer coef ficient with the temperature. Patil et al. [8] characterized numeri cally and experimentally the gas dispersion in a single bubble rising in a fluidized bed. Their simulation showed similar results to the model by Davidson and Harrison [2]. More recently, Solim ene et al. [6] employed a novel technique based on zirconia oxygen sensors to study the nitrogen mixing in a bubble injected in an air fluidized bed, and Pavlin et al. [9] measured the gas interchange in a three dimensional (3D) fluidized bed by means of nuclear mag netic resonance. Though these new experimental methods can ad vance the understanding of the gas transport in a bed, they are still unable to provide a full characterization of the gas interchange be tween the emulsion phase and the bubbles.

Information from experiments can be complemented with pre dictions given by simulations. At this regard, numerical modeling of fluidized bed systems has advanced significantly over the last decades, the most popular modeling approaches being the Euleri an Eulerian [10] and the Eulerian Lagrangian [11] models. In the development and application of these techniques, careful valida tion with either experimental data or theoretical models is re quired [12]. As a result, several reports have appeared in this field comparing the simulation results with experimental data in different regimes and operative conditions such as solids hold up distribution and circulation patterns [13], bubble behavior in a two dimensional (2D) bed [14], solids velocity and bubble characteristics in 2D fluidized beds [15,16], bubble behavior in 3D fluidized beds [17], and pressure drop and bubble behavior in vibrated fluidized beds [18].

In the Eulerian Lagrangian modeling approach the particles are treated as single entities, whose motion is governed by Newton's second law. A Lagrangian simulation of each particle trajectory is coupled with an Eulerian simulation of the bulk gas flow. The inter action between the solid (viz. particles) and gaseous phases is com puted through semi empirical closure models [19]. Although quite promising, this Eulerian Lagrangian approach is very computa tionally expensive and is, therefore, currently unable to simulate the vast number of particles encountered in medium or large scale fluidized beds.

In the two fluid modeling of fluidized beds [10,20] the gas and solid phases are treated as two interpenetrating continua using the conservation equations of fluids. As in the case of the Eulerian Lagrangian approach, the two fluid simulation of fluidized beds re quires the use of closure models for the gas solid interaction. However, since the particle motion is not modeled in detail, the two fluid model also requires closure models to account for the particle particle interactions. These closure relationships may be empirical in nature or based on theoretical relations that are linked to the kinetic theory of gases through the concept of granular tem perature [10].

The aim of the present work is to study the gas interchange due to advection between bubble and emulsion phases in bubbling beds of Geldart B particles. This is done by means of two fluid model simulations in a 2D domain. In the studied beds the bubbles are slow, which means that the advection transport of gas through the bubble boundary is the main mechanism of gas interchange. The first part of the analysis is focused on the behavior of the air through isolated bubbles rising in the bed. This includes the eval uation of the gas pressure distribution and the gas interchange coefficient. The results are compared with the classical potential flow theory by Davidson and Harrison [2]. The isolated bubbles analyzed show, qualitatively and quantitatively, a good agreement with the theory.

Subsequently, the work analyzes the gas interchange in a fluid ized bed operated in bubbling regime, that is, a bed containing multiple interacting bubbles. In addition to the gas interchange coefficient, the crossflow ratio of the bubbles is also evaluated. Both the interchange coefficient and the crossflow ratio in a

bubbling bed are characterized in this work as a function of the bubble size, the distance to the distributor, the superficial gas velocity, and the particle size.

The results indicate that, when the bed is operated in bubbling regime, the potential flow theory for isolated bubbles is no longer valid. Therefore, in order to model the dependence of the gas inter change on the bubble size and superficial velocity, an analytical expression for the gas interchange in multiple interacting 2D bub bles is deduced and compared with the simulation results.

2. Simulated systems

Two different fluidized bed configurations are studied in this work. Table 1 summarizes the general parameters of these two configurations. Configuration 1 was chosen to match the experi mental system and the simulations reported by Patil et al. [8]. Their system was operated under minimum fluidization velocity and an isolated bubble was injected near the distributor. Patil et al. [8] analyzed the consistence of the simulation with the well known potential flow model of Davidson and Harrison [2] as well as with the experimental data. Configuration 2 is a bed arbitrarily selected to carry out the simulations of isolated bubbles as well as multiple interacting bubbles. In all the configurations, air properties at ambient conditions ($T = 20\ ^\circ C$ and $P = 1$ atm) are used for the gas of fluidization and the injection of bubbles. As shown in Table 2, Configuration 1 and 2 were used in case 1 a and case 1 b, respec tively, for the simulation of isolated bubbles injected in a bed flu idized with air at minimum fluidization conditions $U = U_{mf}$. Cases 2 a to 2 h in Table 3 refer to Configuration 2 in fully bubbling con ditions $U \geqslant 1.5U_{mf}$. Case 2 a will be taken as the base case for the characterization of the gas interchange in bubbling fluidized beds. Two different types of Geldart B particles were used in the simula tions. The first type has a particle diameter of $d_p = 0.46$ mm, den sity of $\rho_s = 2660$ kg/m^3 and a resulting minimum fluidization velocity of $U_{mf} = 0.19$ m/s [8]. The second type of particles used in this work has a diameter of $d_p = 0.7$ mm, density of $\rho_s = 2500$ kg/ m^3 and minimum fluidization velocity $U_{mf} = 0.35$ m/s.

Fig. 1 shows two example snapshots of the solids volume frac tion corresponding to the simulation of an isolated bubble using Configuration 1 (case 1 a), and a bubbling bed employing Configu ration 2 (case 2 a). A Cartesian coordinate system is utilized in this work, with the x and y axes are aligned along the horizontal and vertical directions respectively.

Table 1
Simulation configurations.

Parameter	Configuration 1	Configuration 2
Gas density (kg/m^3), ρ_g	1.2	1.2
Gas viscosity (Pa s), μ_g	1.8e−5	1.8e−5
Bed width (m), W	0.3	0.5
Bed walls height (m), H	1	1
Initial voidage (–), $\alpha_{g,i}$	0.4	0.4
Restitution coefficient (–), e	0.95	0.9
Angle of internal friction (°)	30	30

Table 2
Isolated bubble cases.

Case	U/U_{mf}	Static bed height (m), H_0	Particle density (kg/m^3), ρ_s	Particle diameter (mm), d_p	Configuration
1-a	1	0.4	2660	0.46	1
1-b	1	0.5	2500	0.7	2

Table 3
Bubbling regime cases.

Case	U/U_{mf}	Static bed height (m), H_0	Particle density (kg/m^3), ρ_s	Particle diameter (mm), d_p	Configuration
2-a	2.25	0.3	2500	0.7	2
2-b	1.5	0.3	2500	0.7	2
2-c	2.5	0.3	2500	0.7	2
2-d	2.75	0.3	2500	0.7	2
2-e	3	0.3	2500	0.7	2
2-f	2.25	0.15	2500	0.7	2
2-g	2.25	0.5	2500	0.7	2
2-h	2.25	0.3	2660	0.46	2

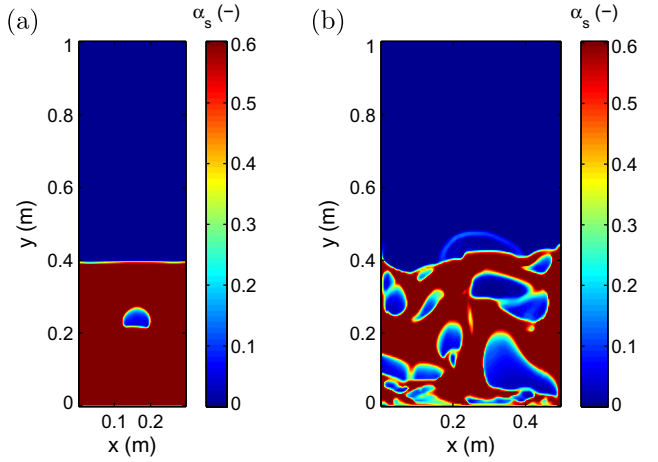

Fig. 1. Snapshot of solids volume fraction for: (a) case 1-a, and (b) case 2-a.

3. Theory

3.1. Two fluid model

The two fluid model is based on the conservation equations of mass, momentum and granular temperature, which were solved here using the MFIX code (Multiphase Flow with Interphase eX changes) [21,22]. The kinetic theory of granular flow, which char acterizes the stochastic fluctuations of the solids kinetic energy, was used for the closure of the solids pressure and stress terms. The governing equations are summarized in the following lines.

Mass conservation of the gas (g) and solid (s) phases:

$$\frac{\partial}{\partial t}(\alpha_g \rho_g) + \nabla \cdot (\alpha_g \rho_g \vec{v}_g) \quad 0 \tag{1}$$

$$\frac{\partial}{\partial t}(\alpha_s \rho_s) + \nabla \cdot (\alpha_s \rho_s \vec{v}_s) \quad 0 \tag{2}$$

Momentum conservation of the gas and solids phases:

$$\frac{\partial}{\partial t}(\alpha_g \rho_g \vec{v}_g) + \nabla \cdot (\alpha_g \rho_g \vec{v}_g{}^2) \quad \alpha_g \nabla p + \nabla \cdot \overline{\overline{\tau_g}} + \alpha_g \rho_g \vec{g} \quad K_{gs}(\vec{v}_g \quad \vec{v}_s) \tag{3}$$

$$\frac{\partial}{\partial t}(\alpha_s \rho_s \vec{v}_s) + \nabla \cdot (\alpha_s \rho_s \vec{v}_s{}^2) \quad \alpha_s \nabla p \quad \nabla p_s + \nabla \cdot \overline{\overline{\tau_s}} + \alpha_s \rho_s \vec{g} + K_{gs}(\vec{v}_g \quad \vec{v}_s) \tag{4}$$

Granular temperature, Θ, balance equation:

$$\frac{3}{2}\left(\frac{\partial}{\partial t}(\rho_s \alpha_s \Theta) + \nabla \cdot (\rho_s \alpha_s \vec{v}_s \Theta)\right) \quad (\quad p_s \bar{\bar{I}} + \overline{\overline{\tau_s}}) : \nabla \vec{v}_s + \nabla \cdot (k_\Theta \nabla \Theta) \quad \gamma_\Theta \quad 3K_{gs}\Theta \tag{5}$$

where p_s is the solids pressure, $\overline{\overline{\tau_i}}$ $\alpha_i\mu_i(\nabla\vec{v}_i + \nabla\vec{v}_i^T) + \alpha_i(\lambda_i - \frac{2}{3}\mu_i)\nabla\cdot\vec{v}_i\bar{\bar{I}}$ is the strain tensor for phase i, $(-p_s\bar{\bar{I}} + \overline{\overline{\tau_s}}):\nabla\vec{v}_s$ is the generation of Θ by the solids stresses, $k_\Theta\nabla\Theta$ is the diffusion of Θ, γ_Θ is the collisional dissipation of Θ and $3K_{gs}\Theta$ is the transfer of random kinetic energy between the solids and the gas. The closure expressions selected for the model are described in [22].

Regarding the numerical solution of the governing equations, a second order accurate scheme was used to discretize the convective derivatives. For case 1 a, the 2D computational domain was discretised using square cells of 5 mm length, in a mesh of 12,000 nodes. For the case 1 b the cells were rectangular with 5 mm length in the x direction and 5.5 mm in the y direction, resulting in a mesh of 18,000 nodes. In all the cases, the time step was automatically adapted to ensure convergence of the equation system and the initial time step was set to 0.5×10^{-5} s at the startup of the simulation. A uniform and steady gas velocity profile was selected for the inlet boundary representing the distributor at the bottom of the bed. A fixed pressure boundary condition was chosen for the top of the freeboard. The lateral walls of the bed were modeled as no slip walls for the gas phase. The Johnson & Jackson partial slip boundary condition were chosen for the solids phase at the walls [23]. The initial solids volume fraction of the bed was set to 0.6.

For the analysis of isolated bubbles in cases 1 a and 1 b, the superficial velocity of the gas that enters the bed was equated to U_{mf}. A void region of square section was set at the bottom of the bed as initial condition. The rest of the emulsion phase was initially at $\alpha_{g,i}$ in Table 1. After a few time steps the bubble is formed and tracked over the time until it reaches the bed surface. The bubbles tested experienced only a small growth along its ascending path. Several simulations starting with different areas of the initial void region were created to produce bubbles of different diameters. For the simulation of the bubbling beds in cases 2 a to 2 h, no injection was needed since bubbles were produced naturally from the fluidization air.

3.2. Drag force

The drag force correlation used in this study for all the simulations is the one proposed by Gidaspow [10]. In this correlation the gas–solid momentum exchange coefficient is defined as:

$$K_{gs} \quad \left\{ \begin{array}{ll} \frac{3}{4}C_D\frac{\rho_g\alpha_g\alpha_s|u_g - u_s|}{d_p}\alpha_g^{-2.65}, & \alpha_g \geqslant 0.8 \\ \frac{150\alpha_s(1-\alpha_g)\mu_g}{\alpha_g d_p^2} + \frac{1.75\rho_g\alpha_s|u_g - u_s|}{d_p}, & \alpha_g < 0.8 \end{array} \right\} \tag{6}$$

where C_D is the dimensionless drag force, which is expressed as a function of the particle Reynolds number $Re = (\rho_g\alpha_g|v_g - v_s|d_p)/\mu_g$:

$$C_D \quad \left\{ \begin{array}{ll} \frac{24}{Re}(1 + 0.15Re^{0.687}), & Re < 1000 \\ 0.44, & Re \geqslant 1000 \end{array} \right\} \tag{7}$$

3.3. Gas interchange parameters

In a gas fluidized bed the gas interchange between bubble and emulsion phases is commonly characterized through the interchange coefficient and the crossflow ratio [1]. The interchange coefficient refers to the volumetric flow rate of gas going from a bubble to the emulsion or from the emulsion to a bubble, $\dot{V}_{be}$, and is expressed per unit volume of the bubble, V_b:

$$K_{be} \quad \frac{\dot{V}_{be}}{V_b} \tag{8}$$

For slow moving bubbles, the integral for the gas flow going from the emulsion phase to a bubble can be considered similar to the integral for the gas flowing from the bubble to the emulsion phase, since bubble coalescence and growth are relatively slow phenomena compared to the gas velocity. In the studied beds the bubbles have a slow rise velocity, which means that the advection transport of gas through the bubble boundary is the main mechanism of gas interchange. For particles smaller than the ones studied in the present work, the bubbles may not be slow and the diffusion of species may play an important role in the gas interchange.

The classical potential flow theory for fluidized beds [2] dictates that 2D isolated bubbles, far from the walls and the bed surface, have an incoming volumetric gas flow rate that is $\dot{V}_{be} \quad 2D_bU_{mf}Z$, with Z as an arbitrary thickness associated to the 2D bed, so that:

$$K_{D\&H,2D} \quad \frac{8U_{mf}}{\pi D_b} \tag{9}$$

Fig. 2 shows a sketch of a bubble and the volume of gas going from the emulsion to the bubble, and from the bubble to the emulsion phase. The bubble velocity in the figure is defined using the displacement of the bubble centroid.

The crossflow ratio accounts for the number of times the bubble gas is replaced as the bubble rises through a characteristic distance, L_c, in the bed:

$$X_{L_c} \quad \frac{K_{be}L_c}{v_b} \tag{10}$$

Here, the characteristic distance can be taken as either the bubble diameter or the vertical distance from the bubble centroid to the average level of the bed surface under bubbling conditions. In Eq. (10) v_b is the bubble rise velocity, which can be estimated for bubbling beds as [1]:

$$v_{b,b} \quad c_1(U - U_{mf}) + c_2\sqrt{gD_b} \tag{11}$$

where c_1 and c_2 are constants that depend on the bed system.

A theoretical value of the crossflow ratio for an isolated bubble can be calculated from the potential flow theory by substituting $K_{D\&H,2D}$ into K_{be}:

$$X_{D\&H,2D} \quad \frac{8U_{mf}L_c}{\pi D_b v_{b,i}} \tag{12}$$

where $v_{b,i}$ is the bubble velocity of an isolated bubble rising in a fluidized bed [2].

$$v_{b,i} \quad \phi\sqrt{gD_b} \tag{13}$$

As first approximation, this expression for isolated bubbles can also be used for bubbling beds [24]. The value of the coefficient ϕ is normally comprised within the interval 0.6 and 1 [1].

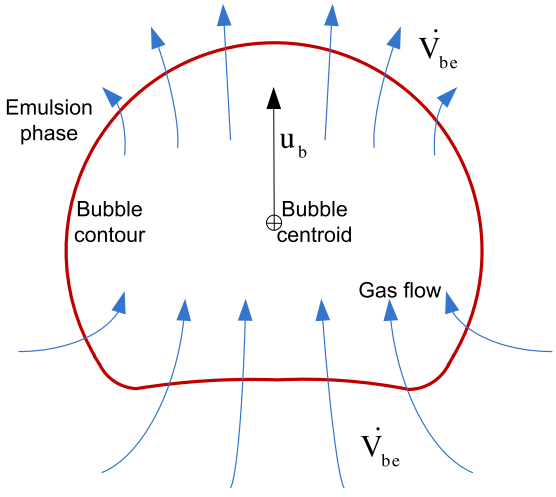

Fig. 2. Sketch of a bubble and the volume of gas going in and out of the bubble.

3.4. Data process technique

To characterize the bubble behavior and calculate the gas inter change, the data from the two fluid simulation were sampled every 5×10^{-3} s over 30 s of physical time. Each instantaneous sample constitutes a frame. To construct mean quantities, the first 5 s at the start up of the simulation were eliminated from the sam pling data set.

In order to study bubble motion, it is necessary to distinguish between bubble and emulsion phases. This is done by setting in a cutoff value equal to $\alpha_s = 0.3$ for the instantaneous solids volume fraction, as reported by Hernández Jiménez et al. [16], which is the arithmetic mean of the maximum and minimum solids volume fractions in the simulated bed. The contour given by the cutoff va lue defines the bubble interphase or boundary. Any region in which the solids volume fraction is less than 0.3 is assigned to be a bub ble. The bubble centroid is the geometrical center of the bubble area delimited by this contour, and the bubble diameter is ob tained from a circle having the same area as the bubble. The bubble velocity is calculated tracking the bubble centroid along consecu tive simulation time steps. Over 70,000 bubbles are extracted for each case to create the time average results.

Once a bubble is defined, the volume of gas going from the bub ble to the emulsion phase (or viceversa) can be calculated. This is done by computing the bubble velocity using two successives frames. Then, the gas flow can be obtained with the gas velocity that is entering or leaving the bubble through its boundary, in a reference system that moves with the bubble:

$$\dot{V}_{be} \quad \int_{\Omega_b} \alpha_g [\ (u_g \quad u_b)dy + (v_g \quad v_b)dx] \tag{14}$$

where u_g and v_g are the horizontal and vertical components of the gas velocity, respectively, u_b and v_b are the horizontal and vertical components of bubble velocity, respectively, and Ω_b is the bubble contour line. To integrate Eq. (14) numerically, the bubble contour Ω_b is divided into small sections $\Omega_{b,k}$. The integral accounting for all the sections $\Omega_{b,k}$ is the net gas flow through the bubble inter phase or boundary, which is null if the bubble growth is much less than the gas interchange (a valid assumption for slow bubbles). Therefore, Eq. (14) must be separated in two contributions, one is the gas going from the emulsion to the bubble ($\dot{V}_{be} > 0$) and the other is the gas going from the bubble to the emulsion ($\dot{V}_{be} < 0$). Thus, for a given bubble, results for all the contour sections, $\Omega_{b,k}$, with positive contributions of the incoming flow, $\dot{V}_{be,k} > 0$, are added (note that these sections may happen to be anywhere at the bubble contour and are not necessarily placed one after the other). The same is done for all the sections through which the flow leaves the bubble, $\dot{V}_{be,k} < 0$. The gas interchange calculated with the incoming flow of a bubble (i.e. summation of each $\dot{V}_{be,k}$ that has po sitive value) is practically identical to the one derived from the out going flow (summation of each $\dot{V}_{be,k}$ that has negative value).

The gas interchange is calculated through the bubble contour, which is not necessarily circular but, instead, kidney shaped or cir cular with a bottom indentation. In contrast, the potential flow theory from Davidson and Harrison [2] simplifies the bubble shape to a perfect circle (in two dimensions). However, Collins [25] dem onstrated that the distortion of the bubble contour introduced by the bottom indentation of a two dimensional bubble have little ef fect on the gas flow field. This probably explains why the simula tion results (pressure profile and gas interchange) for kidney or indented circle shaped isolated bubbles are very close to the re sults estimated using the Davidson and Harrison model [2], as will be shown in Section 4.

Note that the volume of gas going in and out of the bubble, can be calculated using in Eq. (14) the local velocity of the bubble boundary instead of the bubble centroid velocity (u_b, v_b). By this way the effect of the bubble deformation and growth on the gas interchange coefficient can be captured. This boundary velocity can be estimated with the length of a line that perpendicularly leaves the bubble contour from a point at a given frame, and inter sects the contour of the bubble at the following frame. Dividing the length of this line by the time step between the two frames, gives an estimation of the local velocity of the bubble interphase. The boundary velocity, which may not be equal to the solids velocity, is used to evaluate the gas flow that is actually crossing the bubble boundary, that is, the gas velocity relative to the local velocity of the bubble interphase. Therefore, since the gas flow crossing the boundary must be computed with the gas velocity component per pendicular to the bubble boundary, the component of the bubble interphase velocity to be used must be also in perpendicular direc tion to the bubble boundary. Hence, this boundary velocity is not strictly the bubble centroid velocity, though it can be demonstrated that the these two velocities leads to consistent results, that is, they produce similar values of the gas interchange through a non grow ing bubble if the time step used in the calculation of the boundary velocity is small. For size or shape varying bubbles, the use of the local velocity of the bubble boundary provides a more accurate va lue for the volume of gas crossing the bubble, but the computational cost is dramatically increased. For the isolated bubble and the bub bling regime cases studied in the present work, several tests were done using the boundary velocity of the bubble (for the isolated bubble and for the bubbling regime cases), and results similar to those using the centroid velocity of the bubble were obtained. This outcome should be expected since the observed bubble displace ment and deformation is relatively slow compared to the intersti tial gas velocity. Therefore, from hereafter it is implicit that all the results presented were calculated using the bubble centroid veloc ity (u_b, v_b) in Eq. (14), as the associated computational cost is lower.

4. Results for isolated bubbles

4.1. Pressure distribution

The first part of the analysis is devoted to a practical validation of the simulated gas behavior through isolated bubbles. For this pur pose, the gas pressure recovery and distribution for an isolated ris ing bubble is studied using cases 1 a and 1 b of Table 2. Fig. 3 shows the pressure signal for an acquisition point placed at the middle of the bed at a height above the distributor $y = 0.2475$ m. This point is crossed by a rising isolated bubble producing a variation of the local pressure of the gas over the time shown in Fig. 3a. The temporal evolution of the pressure experiences a rapid fall, indicating that the bubble crosses the acquisition point at a time between 0.4 and 0.5 s after having been injected. The pressure is recovered once the bubble has crossed the acquisition point.

The pressure distribution obtained from the simulation in the vicinity of a rising 2D bubble (case 1 a) is included in Fig. 3b. In this figure the vertical axis y_c is the vertical coordinate relative to the bubble centroid while ΔP_g is the gas pressure, also relative to the pressure at the bubble centroid. As Fig. 3b shows, the presence of the bubble perturbs the linear decay given by the solids column weight (i.e. $y_c \rho_d g$) creating an overpressure over the bubble and a pressure depression at the bubble wake. To verify the validity of this simulation outcome the pressure distribution from the potential flow model for a cylindrical void [2] is plotted in Fig. 3b:

$$\frac{\Delta P_g}{\rho_d} \quad \left\{ \begin{array}{c} g\left(y_c \quad \frac{a^2}{y_c}\right), \quad |y_c| \geqslant a \\ 0, \quad |y_c| < a \end{array} \right\} \tag{15}$$

where a is the radius of the bubble and $\rho_d = \alpha_g \rho_g + (1 \quad \alpha_g)\rho_s$ is the bulk density of the emulsion phase. As can be observed, the

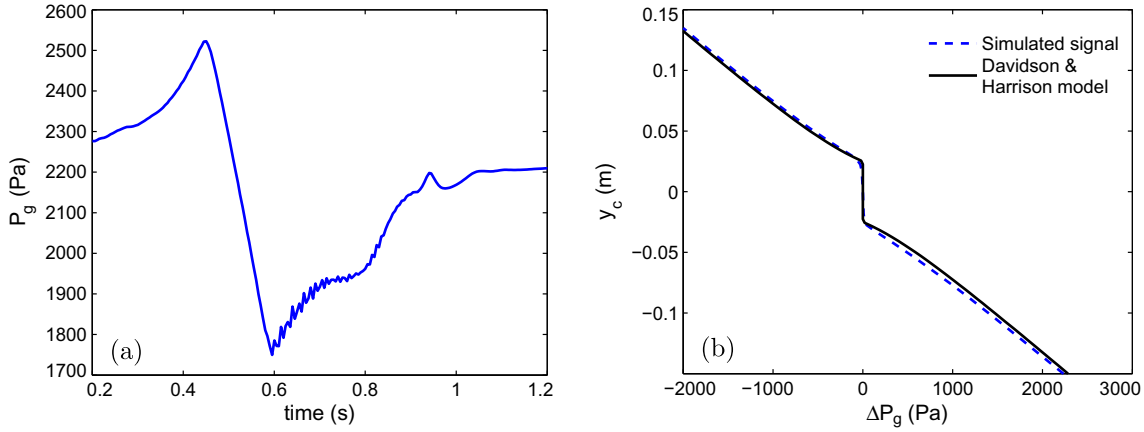

Fig. 3. (a) Simulated gas pressure signal versus time at a height of $y = 0.2475$ m perturbed by a bubble, and (b) gas pressure distribution along the radial coordinate with the theoretical model by Davidson and Harrison. Case 1-a.

pressure distribution in the vicinity of an isolated bubble in the simulation fits fairly well the theoretical potential flow model.

4.2. Gas interchange

Once the pressure perturbation produced by an isolated bubble has been verified, the gas interchange between isolated bubbles and the emulsion phase can be studied and compared with the potential flow model by Davidson and Harrison [2]. To fulfill this goal, several isolated bubbles in cases 1 a and 1 b were simulated.

Fig. 4 shows the gas interchange coefficient obtained from the two fluid model simulations for several isolated bubbles injected in a bed of particles with diameter $d_p = 0.46$ mm Fig. 4a and $d_p = 0.7$ mm (Fig. 4b). Each bubble produces a set of scatter points corresponding to the evolution of the instantaneous interchange coefficient from the formation of the bubble until the eruption at the bed surface. Bigger bubbles are formed farther from the distributor, requiring less time to erupt and, therefore, fewer data points in the figure are obtained in that case. In Fig. 4 the interchange coefficient calculated from the potential flow model proposed by Davidson and Harrison [2] is included. As can be seen, all the bubbles are in very good agreement with the potential flow model, Eq. (9). Excellent agreement between simulated isolated bubbles and the potential flow theory was also reported by Patit et al. [8] in a bed similar to the one used in Fig. 4a (case 1 a).

The results of this section indicate that the two fluid simulation can reproduce realistically the gas flow and pressure distribution through isolated bubbles in accordance to the potential flow theory. Besides, previous works have shown that the solid motion in the vicinity of bubbles obtained from two fluid simulations also follows the theoretical velocity given by the potential flow model [26].

5. Results for fully bubbling beds

5.1. General bubble behavior

Before analyzing the gas interchange in fully bubbling beds, this part of the analysis concentrates on the general behavior of bubbles in the bed simulated in case 2 a. Fig. 5 shows the mean bubble diameter D_b and the vertical bubble velocity v_b, as a function of the height above the distributor, y, and the bubble diameter, D_b. Fig. 5b also includes two models for the bubble velocity. One model is given by Eq. (13) using the typical value $\phi = 0.7$. The other model is Eq. (11) whose coefficients $c_1 = 0.48$ and $c_2 = 0.53$ have been obtained by regression fitting of the model to the simulation results.

Fig. 5 depicts the typical behavior of bubbles that takes place in a 2D bubbling bed. The black solid curve in Fig. 5 is the mean of the bubble data set, calculated for each interval of the horizontal axis of the plots, and the vertical errorbars refer to plus/minus one standard deviation of the data. The cross points correspond to

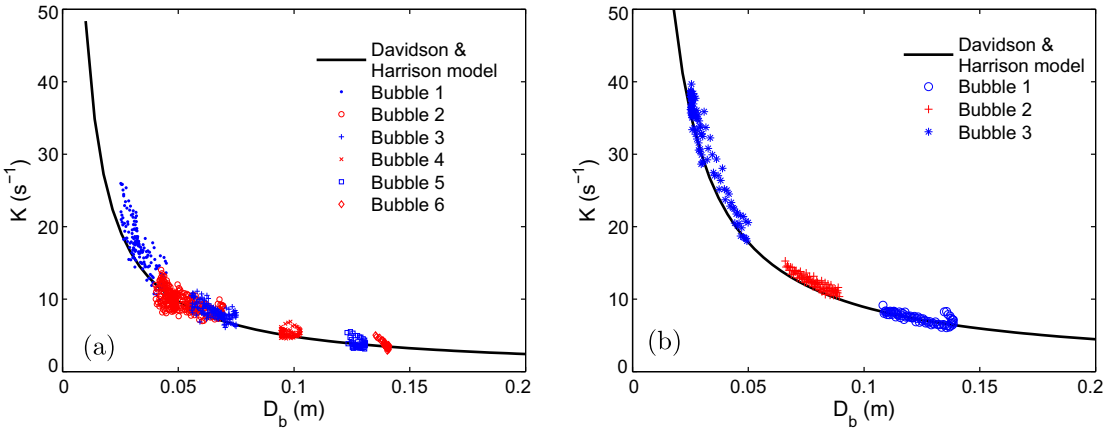

Fig. 4. Interchange coefficient versus the bubble diameter for several isolated bubbles and comparison with the model by Davidson and Harrison, (a) particles with $d_p = 0.46$ mm (case 1-a); and (b) particles with $d_p = 0.7$ mm (case 1-b).

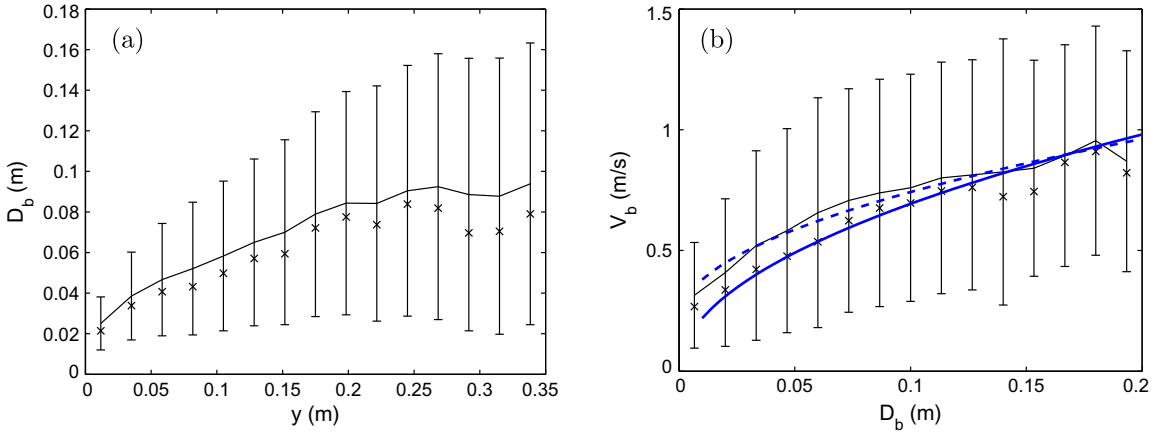

Fig. 5. (a) Bubble diameter versus height above the distributor and (b) bubble velocity versus bubble diameter. Case 2-a. Black solid line: mean and standard deviation values, ×: median values. Blue solid line: v_b $0.7\sqrt{gD_b}$. Blue dashed line: v_b $0.48(U - U_{mf}) + 0.53\sqrt{gD_b}$. (For interpretation of the references to color in this figure legend, the reader is referred to the web version of this article.)

the median of the data. It can be observed that both median and mean values give very similar results in Fig. 5. The bubble diameter increases monotonically with the height above the distributor (Fig. 5a). As expected, the bubble velocity shown in Fig. 5b in creases with the bubble diameter. These results on the bubble behavior are in harmony with experimental measurements, as pre viously reported [14 16]. Fig. 5b indicates that the mean bubble velocity is slow. This is so since the bubble velocity remains below the gas interstitial velocity ($U_{mf}/\alpha_{g\ m\ f} \approx$ 0.87 m/s). Only large bub bles seem to have mean velocity greater than the interstitial veloc ity (Fig. 5b).

5.2. Mean interchange coefficient and crossflow ratio

The mean interchange coefficient and the crossflow ratio are studied in this section. As shown in Section 4.2, the simulations are able to predict the gas interchange of isolated bubbles accord ing to the theoretical model by Davidson and Harrison [2]. How ever, this theoretical model of potential flow was developed for isolated bubbles and does not consider the perturbation arising from the interaction between two or more bubbles. Consequently, a new model is developed here in order to incorporate this interac tion between bubbles in the estimation of the gas interchange.

When slow bubbles are close to each other, the excess gas passes through bubbles as a low resistance shortcut to the free board [1]. The larger the superficial velocity in the bed, the greater the number of bubbles and the more intense the gas flow through the bubbles, the so called throughflow, which plays an important role in bubbling fluidized beds and should be taken into account. The throughflow velocity U_{th} can be estimated as the excess of gas velocity (U U_{mf}) that is not transported by the visible flow of bubbles and concentrates preferentially in the bubble path re gions. The effect of the throughflow on the gas interchange was first studied by Sit and Grace [4]. They measured the interphase mass transfer for a pair of coalescence bubbles, and estimated a rough enhancement factor based on the percentage of the bubbles coalescing in a freely bubbling bed.

In the present work a different approach from that of Sit and Grace [4] is followed. It will be assumed that the presence of multi ple interacting bubbles in a bed increases the gas velocity in the vicinity of each bubble. An effective way of considering this effect is to use a corrected velocity U^* in the Harrison and Davidson's interchange coefficient, Eq. (9), in place of the minimum fluidiza tion velocity U_{mf}. The corrected velocity U^* comprises the through flow velocity as well as the minimum fluidization velocity:

$$U^* \quad U_{mf} + U_{th} \quad U_{mf} + \delta(1 \quad \Psi)(U \quad U_{mf}) \tag{16}$$

where δ is the throughflow concentration parameter, which is just the fraction of the bed where the gas velocity modulus (i.e. magni tude) is higher than the interstitial minimum fluidization velocity U_{mf}/α_g. The estimation of δ in the 2D simulated bed can be done as follows. Fig. 6 shows a snapshot of the bed containing the bubble

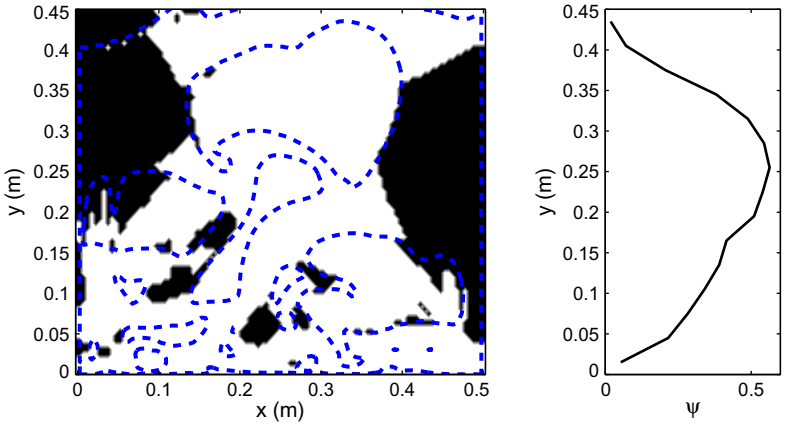

Fig. 6. Snapshot of the bed with black areas as the region with a gas velocity below the interstitial gas velocity, and time-averaged coefficient Ψ as a function of the height. Case 2-a.

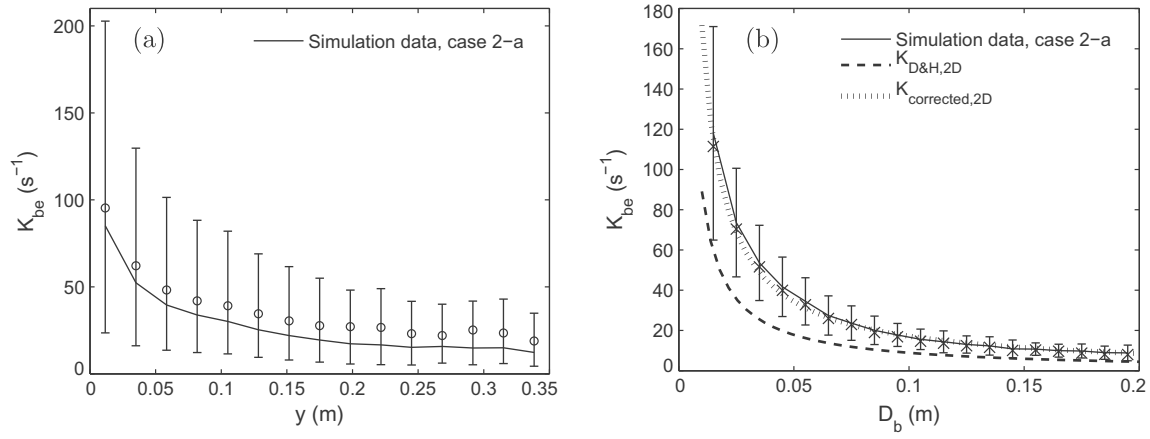

Fig. 7. Gas interchange coefficient (a) versus the height, solid line: median values and interquartile ranges, ∘: mean values; and (b) versus the bubble diameter together with the theoretical model by Davidson and Harrison and the corrected model, Eq. (19), solid line: mean and standard deviation values, ×: median values. Case 2-a.

and surface contours. The area in black color, A_1, corresponds to the regions of the bed (taken only those below the bed surface) where the gas velocity is smaller than U_{mf}/α_g, and the area in white color, A_2, is the area where the gas velocity is greater than U_{mf}/α_g. The instantaneous value of the throughflow concentration parameter is then $\delta_k = (A_1 + A_2)/A_2$, and the time average value of δ_k, covering all the simulation time, provides δ. For the base case (case 2 a), the simulation results give $\delta = 1.30$.

Ψ in Eq. (16) is the fraction of the visible flow over the excess flow, i.e. visible flow over that predicted by the two pahse theory. The visible flow can be calculated for each time instant as the apparent volumetric flow rate that is transported by the bubbles crossing a given sampling horizontal section in the bed.

$$\Psi \quad \sum_{i \in bubbles} \frac{v_{b,i}\pi D_{b,i}^2/4}{(U \quad U_{mf})WH} \tag{17}$$

The time average profile of Ψ is presented in Fig. 6 as a function of the distance of the sampling horizontal section to the bed distribu tor, y. The mean of Ψ along y in Fig. 6 gives $\Psi = 0.394$ for case 2 a.

Therefore, introducing U^* from Eq. (16) in Eq. (9) leads to the following correction of the interchange coefficient:

$$K_{corrected,2D} \quad \frac{8U^*}{\pi D_b} \quad \frac{\zeta U}{D_b} \tag{18}$$

where $\zeta = (8/\pi)[\delta(1 \quad \Psi) + (U_{mf}/U)(1 \quad \delta \quad \delta\Psi)]$. Using the values for δ and Ψ calculated before for case 2 a, it is easy to see that $\zeta = 2.246$. For the sake of simplicity and compactness, ζ can be approximated to 9/4. Thus:

$$K_{corrected,2D} \approx \frac{9U}{4D_b} \tag{19}$$

The mean interchange coefficient K_{be} is presented in Fig. 7 and has been calculated making the average of the individual interchange coefficient of the simulated bubbles within each interval of vertical distance to the distributor (horizontal axis in Fig. 7a) or bubble diameter (Fig. 7b). In Fig. 7a the median and the interquartile ranges are plotted, with circles denoting the mean values. In this case the median is not equal to the mean value since the values of the interchange coefficient at each vertical distance do not follow a nor mal distribution. In Fig. 7b, the mean and standard deviation are de picted as a continuous line plus the errorbars, and the median as cross points. As can be observed in Fig. 7b, both mean and median values give similar values when plotted versus the mean bubble diameter. Therefore, only the mean value of the interchange coeffi cient will be provided from now on when plotted versus the bubble diameter. Fig. 7b also shows the gas interchange coefficient calcu lated with the model by Davidson and Harrison [2], Eq. (9), and with the corrected model, Eq. (19). Of the two models, the corrected model is the one that best predicts the simulation results for the gas interchange.

According to Fig. 7a, the gas interchange per unit volume reduces when the distance to the distributor increases. This hap pens because the bubble diameter grows with the height, Fig. 5a, while the gas interchange decreases with the bubble diameter, Fig. 7b. The fact that the interchange coefficient decreases with the bubble diameter in Fig. 7b evidences that the gas flow inter changed between dense and bubble phases grows less rapidly than the bubble volume when the bubble diameter increases. In fact, according to the classical potential flow theory, i.e. $K_{D\&H,2D}$ in Eq. (9), the interchange coefficient is inversely propor tional to the bubble diameter. However, it is clear from Fig. 7b that $K_{D\&H,2D}$ is 50% smaller than the interchange coefficient from the two fluid simulations. This is due to the fact that the poten tial flow theory applies to isolated bubbles that are very far from other bubbles.

The value of the coefficient ζ may be also adjusted by fitting Eq. (18) to the two fluid simulation results shown in Fig. 7b. Perform ing this fitting by regression, the value $\zeta = 2.272$ is obtained, which is surprisingly close to the previously deduced value $\zeta = 9/4$.

The expression for the corrected interchange coefficient $K_{corrected}$,2D, Eq. (19), can be used to define a corrected crossflow ratio:

$$X_{corrected,2D} \quad \frac{K_{corrected,2D}L_c}{v_b} \quad \frac{9U}{4D_b v_b} \tag{20}$$

where v_b is the bubble velocity that can be either $v_{b,i}$, or $v_{b,b}$.

Fig. 8 shows the crossflow ratio as a function of the distance above the distributor and as a function of the bubble diameter. In this figure the crossflow ratio has been calculated from the simula tion using the median of the individual crossflow ratios of the bub bles captured within each abscissa interval of distance to the distributor, Fig. 8a, and of bubble diameter, Fig. 8b.

In Fig. 8a, X_{fb} denotes the crossflow ratio computed with the charateristic length, L_c, equal to the distance from the bubble cen troid to the surface of the bed. This crossflow ratio represents the maximum number of times the gas contained in a bubble can be renewed until the bubble reaches the bed surface. When the char acteristic length, L_c, is equal to the bubble diameter, D_b, the cross flow ratio is denoted with X_{Db} and can be interpreted as an approximation of the number of times the bubble gas is renewed between successive bubble coalescences, whose frequency is of

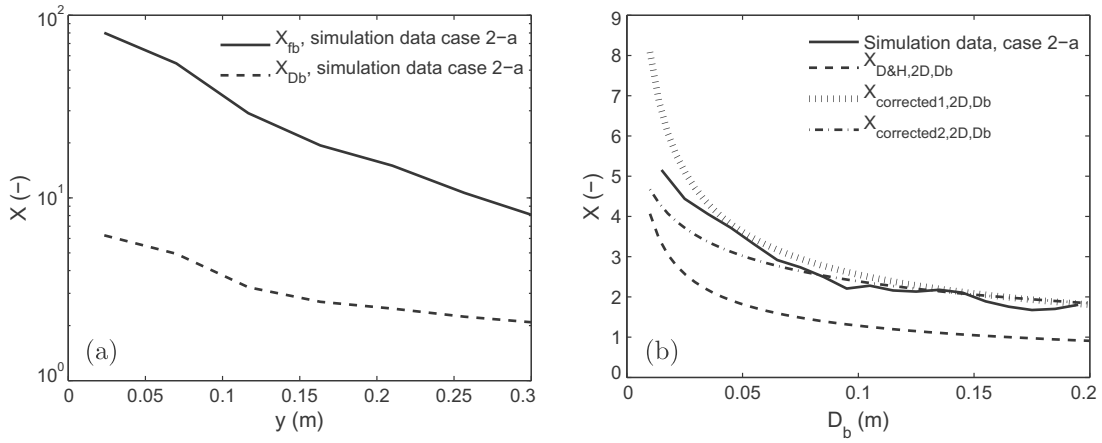

Fig. 8. Crossflow ratio (a) versus the height (using $L_c = fb$ and $L_c = D_b$); and (b) versus the bubble diameter (using $L_c = D_b$) together with the theoretical model by Davidson and Harrison and the corrected model. Case 2-a.

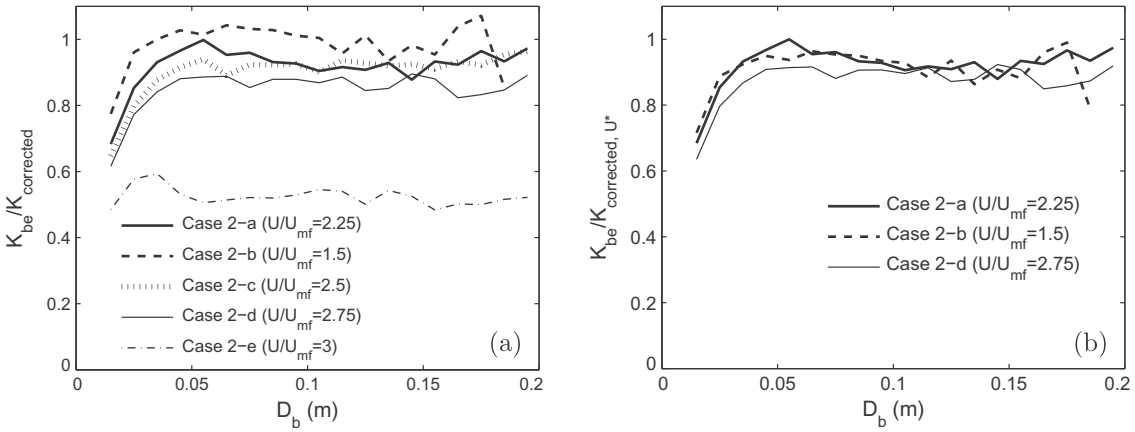

Fig. 9. Normalized interchange coefficient versus the bubble diameter: (a) using $\zeta = 9/4$ for cases 2-a–e; and (b) using U^* for cases 2-a, b, d.

order U_b/D_b in a bed densely populated with bubbles such as the one studied here [24].

According to the above definition, X_{fb} is typically greater than X_{Db}, as Fig. 8 demonstrates, and the two crossflow ratios decrease with the distance to the distributor and the bubble diameter. Interestingly, K_{be} in Fig. 7a and X_{Db} in Fig. 8a, seem to have relatively low sensitivity to the distance to the distributor within a large fraction of the bed ($y/H_0 > 1/3$).

The crossflow ratio X_{Db} obtained from the two fluid simulation of the bubbling bed is shown in Fig. 8b together with the predictions given by the potential flow model, $X_{D\&H,2D}$ in Eq. (12) for $L_c = D_b$, and the corrected crossflow ratio proposed in this work, $X_{corrected,2D}$ for the two approximations concerning the bubble velocity in Eq. (20). One approximation takes the bubble velocity from Eq. (13) with $\phi = 0.7$ to calculate the crossflow ratio, $X_{corrected1,2D}$. The aim of this approximation is to obtain a model as simple as possible. The other approximation uses Eq. (11) with c_1 and c_2 adjusted from the simulation case 2 a (see Fig. 5b) to calculate $X_{corrected2,2D}$. As in the case of the interchange coefficient in Fig. 7b, the potential flow model $X_{D\&H,2D}$ underpredicts the simulated crossflow ratio in Fig. 8b, while the corrected model $X_{corrected,2D}$ better fits the simulation data. In particular, the corrected model using the bubble velocity $v_{b,b}$, $X_{corrected2,2D}$, gives the closest results to the simulated crossflow ratio. Nevertheless, the corrected crossflow ratio, $X_{corrected1,2D}$, can be used as well for simplicity without incoming an excesive error.

5.3. Effect of the superficial gas velocity

This section investigates the effect of the superficial gas velocity on the interchange coefficient. In Fig. 9a the mean gas interchange coefficient has been normalized with the analytical model $K_{corrected,2D}$ given by Eq. (19). The simulations represent bubbling beds with 5 different superficial velocities ranging from $U/U_{mf} = 1.5$ to 3 (i.e. from $U = 0.525$ m/s to 1.05 m/s) and the same settled bed height $H_0 = 0.3$ m (cases 2 a to 2 e).

As Fig. 9a reflects, if bubbles are not very small, all the values of the normalized interchange coefficient are nearly constant and close to the unity despite their different superficial velocity. This demonstrates that the model proposed in Eq. (19) is capable of incorporating the increase of the gas interchange coefficient when the superficial gas velocity is augmented. Exception of this is the gas interchange of bubbles in the bed with the highest superficial velocity, case 2 e (Table 3). Passing from superficial velocity

Table 4
Values of δ, Ψ and ζ for cases 2-a, 2-b and 2-d.

Case	U/U_{mf}	δ	Ψ	ζ
2-a	2.25	1.3	0.3943	2.2463
2-b	1.5	1.45	0.401	2.435
2-d	2.75	1.26	0.385	2.1817

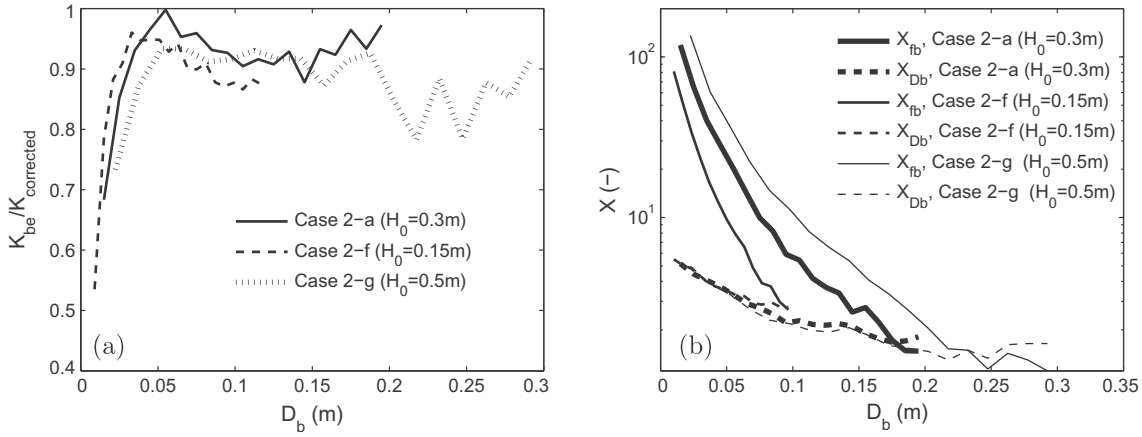

Fig. 10. Effect of the static bed height on: (a) the normalized interchange coefficient; and (b) the crossflow ratio, versus the bubble diameter. Cases 2-a, f, g.

$2.75U_{mf}$ to $3U_{mf}$ abruptly halves the mean gas interchange coeffi cient. This can be explained considering that the air excess of case 2 e gives a regime transition from freely bubbling to turbulent flu idization. The regime transition for superficial velocities $U \sim 3U_{mf}$ has been also reported by Makkawi and Wright [27]. Therefore, the proposed model $K_{corrected,2D}$ can be used when the fluidized bed is working in bubbling regime but not in turbulent fluidization.

Despite $K_{corrected,2D}$ shows a very good adjustment with the simulation results, it can be slightly improved by calculating more precisely ζ in Eq. (18). Varying the superficial gas velocity leads to a change in the coefficients Ψ and δ that may affect ζ and $K_{corrected,2D}$ used for the normalization in Fig. 9a. Table 4 contains the resulting values of δ and Ψ for three different superficial velocities in the simulated bubbling bed (cases 2 a, 2 b and 2 d).

According to Table 4, increasing the superficial velocity U of the bed uniformizes the throughflow within the bed area since δ de creases. The simulations also seem to indicate that the increase of U has the additional effect of augmenting the throughflow in a larger extend than the visible flow, which produces a slight de crease on the value of Ψ. The resulting value of ζ decreases with an increase of U as shown in Table 4. When the values of ζ in Table 4 are incorporated in $K_{corrected,2D}$ Eq. (18) for the normalization of the interchange coefficient, the curves shown in Fig. 9b are less sensi tive to U/U_{mf} than in Fig. 9a. Therefore, the corrected model in Eq. (18) is able to retain more precisely the effect of the superficial gas velocity on the interchange coefficient in a bubbling bed. Neverthe less, the observed variation of ζ with U/U_{mf} is not intense and $\zeta = 9/4$ can be considered a good approximation for the 2D bubbling beds studied here.

5.4. Effect of bed height

The effect of the bed height on the gas interchange between bubbles and emulsion is shown in Fig. 10. This figure contains the normalized interchange coefficient defined previously and the crossflow ratio versus the bubble diameter. Results are de picted for different settled bed heights, H_0, and same superficial gas velocity ($U = 2.25U_{mf}$).

It seems from Fig. 10a that the gas interchange coefficient of a bubble with a given diameter is not strongly affected by the static bed height when the bubble diameter is greater than 5 cm. Obvi ously, the crossflow ratio calculated using the distance to the free board, Fig. 10b, increases with the settled bed height since bubbles require longer times to reach the bed surface. In turn, the crossflow ratio calculated using the bubble diameter, X_{Db}, is not affected by the static bed height, which corroborates the fact that the gas interchange and bubble velocity can be assumed insensitive to the settled bed height for the operating conditions analyzed in this work.

Taking into account the reduced effect of the bed height on the gas interchange, substantial differences in the interchange coeffi cient are not expected when increasing the bed width while keep ing the gas superficial velocity unchanged. However, if the bed width is reduced to values close to the bubble diameter, the bed

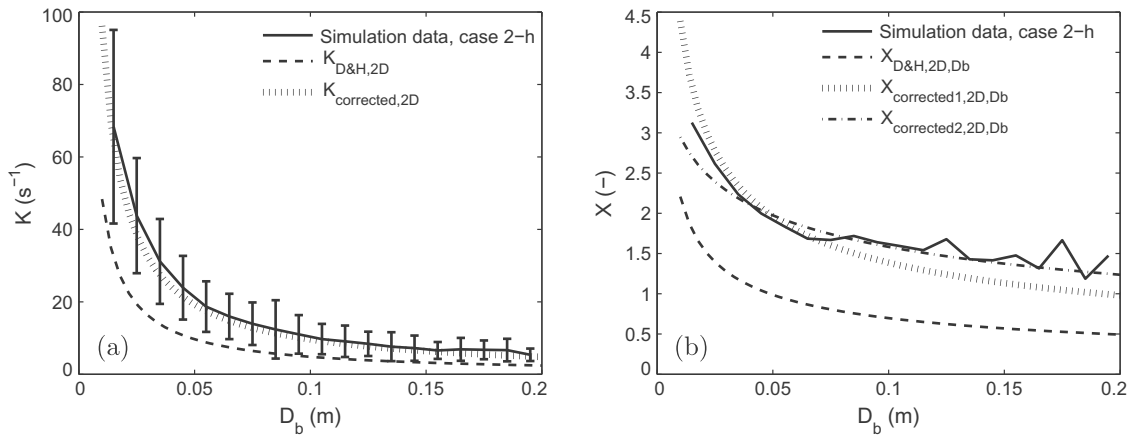

Fig. 11. Results for particles with d_p = 0.46 mm: (a) interchange coefficient; and (b) crossflow ratio, versus the bubble diameter. Case 2-h.

regime passes from bubbling to slugging and significant changes on the interchange coefficient may occur.

5.5. Effect of the particle size

In this section the effect of the particle size is studied with the simulation results from case 2 h in Table 3. In this case, the particles used are smaller (d_p = 0.46 mm) than in case 2 a (d_p = 0.7 mm). The static bed height H_0 = 0.3 m and the relative superficial gas velocity U/U_{mf} = 2.25 was taken the same for the two cases. Note that in case 2 h, the superficial gas velocity U = 0.4275 m/s, is different from case 2 a since U_{mf} depends on the particle size. Fig. 11 shows the simulated interchange coefficient and crossflow ratio, using $L_c = D_b$, for case 2 h. The results are presented together with the theoretical model by Davidson and Harrison [2], Eq. (9), and the corrected model, Eqs. (19) and (20), for the case 2 h.

As reflected in Fig. 11, particles with diameter d_p = 0.46 mm lead to smaller gas interchange coefficients and crossflow ratios than particles with d_p = 0.7 mm (Figs. 7b and 8b). Using smaller particles means that the minimum velocity U_{mf} needed to fluidized the bed is smaller and, therefore, smaller values of the interchange coefficient are obtained. Fig. 11a demonstrates that for particles with d_p = 0.46 mm the corrected model $K_{corrected,2D}$ Eq. (19), is still a good approximation to the gas interchange coefficient calculated from the two fluid 2D simulations of bubbling beds. As in Fig. 7b, $K_{D\&H,2D}$ from the potential flow theory for isolated bubbles clearly underpredicts the interchange coefficient given by the simulations.

Concerning the crossflow ratio shown in Fig. 11b, the corrected model $X_{corrected1,2D}$ was calculated using Eq. (20) with $v_b = v_{b,i}$ and ϕ= 0.7 as in Fig. 8b. $X_{corrected2,2D}$ was obtained employing Eq. (20) with $v_b = v_{b,b}$. In this case the bubble velocity, $v_{b,b}$, was computed by fitting Eq. (11) to the mean bubble velocity obtained from the simulated case 2 h, leading to c_1 = 0.82 and c_2 = 0.41. Differences between $X_{corrected1,2D}$ and $X_{corrected2,2D}$ are relatively small and both approaches give acceptable estimations of the simulated crossflow ratio.

6. Conclusions

Two fluid model simulations were used in this work to characterize the mean gas interchange coefficient K_{be} and crossflow ratio X of bubbles in a fluidized bed of Geldart group B particles.

Firstly, it has been demonstrated that the simulations are able to reproduce realistically the pressure distribution and the gas flow for isolated bubbles, and the results are in agreement with classical potential flow model by Davidson and Harrison [2].

Secondly, the mean gas interchange coefficient K_{be} and cross flow ratio X of slow bubbles in two dimensional fully bubbling beds were characterized for several operating conditions. Both K_{be} and X decrease with the distance to the distributor and the bubble diameter, their values being over two times those predicted by the potential flow theory of isolated bubbles. To improve the prediction of the gas interchange coefficient between bubble and emulsion phases, the corrected expression $K_{corrected,2D} \approx 9U/4D_b$ was proposed in the present work for multiple interacting 2D bubbles. This novel expression is able of predicting the gas interchange coefficient and crossflow ratio, even varying the superficial gas velocity, the static bed height and the particle size. A limitation of the model was found when the fluidized bed is working under high gas velocity rates. In particular, at a velocity of $U \sim 3U_{mf}$, the fluidization regime is transitioning from freely bubbling to turbulent fluidization, and the values predicted by $K_{corrected,2D}$ overestimate those given by the 2D simulation.

It is worth noticing that the value of the gas interchange coefficient for interacting bubbles in 3D bubbling beds is expected to be greater than in 2D bubbling beds, since surface volume ratio for 3D bubbles is greater than the perimeter area ratio for 2D bubbles, an effect also predicted by the potential flow theory for the case of isolated bubbles [2]. Nevertheless, proper estimation of the interchange coefficient would require the simulation of full 3D beds.

The corrected expressions proposed in this work accounting for the gas interchange coefficient and crossflow ratio for 2D bubbles, may be of direct application in the development of discrete bubble models (DBM) and other phenomenological tools used for simulating industrial scale fluidized bed gasifiers and combustors, in which the prediction of the gas behavior is a key factor.

Acknowledgments

This work has been partially funded by the Spanish Government (Project DPI2009 10518) and the Autonomous Community of Madrid (Project S2009/ENE 1660).

References

[1] D. Kunii, O. Levenspiel, Fluidization Engineering, Butterworth-Heinemann, Newton, MA, 1991.
[2] J.F. Davidson, D. Harrison, Fluidized Particles, Cambridge University Press, New York, 1963.
[3] S.P. Sit, J.R. Grace, Interphase mass transfer in an aggregative fluidized bed, Chem. Eng. Sci. 33 (1978) 11115–11122.
[4] S.P. Sit, J.R. Grace, Effect of bubble interaction on interphase mass transfer in gas fluidized beds, Chem. Eng. Sci. 36 (1981) 327–335.
[5] T. Chiba, H. Kobayashi, Gas exchange between the bubble and emulsion phases in gas–solid fluidized beds, Chem. Eng. Sci. 25 (1970) 1375–1385.
[6] R. Solimene, A. Marzocchella, G. Passarelli, P. Salatino, Assessment of gas-fluidized beds mixing and hydrodynamics by zirconia sensors, AIChE J. 52 (2006) 185–198.
[7] W. Wu, P.K. Agarwal, The effect of bed temperature on mass transfer between the bubble and emulsion phases in a fluidized beds, Can. J. Chem. Eng. 81 (2003) 940–948.
[8] D.J. Patil, M.v. Sint Annaland, J.A.M. Kuipers, Gas dispersion and bubble-to-emulsion phase mass exchange in a gas–solid bubbling fluidized bed a computational and experimental study, Int. J. Chem. React. Eng. 1 (2003) 1–20.
[9] T. Pavlin, R. Wang, R. McGorty, M.S. Rosen, D.G. Cory, D. Candela, R.W. Mair, R.L. Walsworth, Noninvasive measurements of gas exchange in a three dimensional fluidized bed by hiperpolarized Xe NMR, Appl. Magn. Reson. 32 (2007) 93–122.
[10] D. Gidaspow, Multiphase Flow and Fluidization: Continuum and Kinetic Theory Descriptions, Academic Press, San Diego, CA, 1994.
[11] Y. Tsuji, T. Kawaguchi, T. Yanaka, Discrete particle simulations of 2-dimensional fluidized-beds, Powder Technol. 77 (1993) 79–87.
[12] J.R. Grace, F. Taghipour, Verification and validation of CFD models and dynamic similarity for fluidized beds, Powder Technol. 139 (2004) 99–110.
[13] G.N. Ahuja, A.W. Patwardhan, CFD and experimental studies of solids hold-up distribution and circulation patterns in gas solid fluidized beds, Chem. Eng. J. 143 (2008) 147–160.
[14] A. Busciglio, G. Vella, G. Micale, L. Rizzutia, Analysis of the bubbling behaviour of 2D gas solid fluidized beds: Part II. Comparison between experiments and numerical simulations via digital image analysis technique, Chem. Eng. J. 148 (2009) 145–163.
[15] T. Li, J.R. Grace, X. Bi, Study of wall boundary condition in numerical simulations of bubbling fluidized beds, Powder Technol. 203 (2010) 447–457.
[16] F. Hernández-Jiménez, S. Sánchez-Delgado, A. Gómez-García, A. Acosta-Iborra, Comparison between two-fluid model simulations and particle image analysis & velocimetry (PIV) results for a two-dimensional gas–solid fluidized bed, Chem. Eng. Sci. 66 (2011) 3753–3772.
[17] A. Acosta-Iborra, C. Sobrino, F. Hernández-Jiménez, M. de Vega, Experimental and computational study on the bubble behavior in a 3-D fluidized bed, Chem. Eng. Sci. 66 (2011) 3499–3512.
[18] A. Acosta-Iborra, F. Hernández-Jiménez, M. de Vega, J.V. Briongos, A novel methodology for simulating vibrated fluidized beds using two-fluid models, Chem. Eng. J. 198–199 (2012) 261–274.
[19] N.G. Deen, M. van Sint Annaland, M.A. van der Hoef, J.A.M. Kuipers, Review of discrete particle modelling of fluidized beds, Chem. Eng. Sci. 62 (2007) 28–44.
[20] B.G.M. van Wachem, A.E. Almstedt, Methods for multiphase computational fluid dynamics, Chem. Eng. J. 96 (2003) 81–98.
[21] M. Syamlal, W. Rogers, T.J. O'Brien, MFIX Documentation: Theory Guide, U.S. Department of Energy (DOE), Morgantown Energy Technology Center, Morgantown, West Virginia, 1993.

[22] S. Benyahia, M. Syamlal, T.J. O'Brien, Summary of MFIX Equations 2005-4, 2007.
[23] P.C. Johnson, R. Jackson, Frictional collisional constitutive relations for antigranulocytes materials with application to plane shearing, J. Fluid Mech. 176 (1987) 67–93.
[24] R.C. Darton, R.D. La Nauze, J.F. Davidson, D. Harrison, Bubble growth due to coalescence in fluidised beds, Trans. IChemE. 55 (1977) 2411–2437.
[25] R. Collins, An extension of Davidson's theory of bubbles in fluidized beds, Chem. Eng. Sci. 20 (1965) 747–755.
[26] F. Hernández-Jiménez, J.R. Third, A. Acosta-Iborra, C.R. Müller, Comparison of bubble eruption models with two-fluid simulations in a 2D gas-fluidized beds, Chem. Eng. J. 171 (2011) 328–339.
[27] Y.T. Makkawi, P.C. Wright, Fluidization regimes in a conventional fluidized bed characterized by means of electrical capacitance tomography, Chem. Eng. Sci. 57 (2002) 2411–2437.